Double-decker CDC-ROADM node for multi-band network with wavelength band granularity

Kenya Suzuki[1*], Masashi Ota[1], Yoshie Morimoto[1], Keita Yamaguchi[1], Fukutaro Hamaoka[2], Shuto Sugawara[2], Takeo Sasai[2], Takayuki Kobayashi[2], Masanori Nakamura[2], Satomi Katayose[3], Takeshi Umeki[3], Daisuke Ogawa[4], Yiran Ma[5], Stefano Camatel[5], Mitsunori Fukutoku[4], Yutaka Miyamoto[2], and Osamu Moriwaki[1]

[1]NTT Device Innovation Center, NTT Corporation, 3-1 Morinosato Wakamiya, Atsugi, Kanagawa 243-0198, Japan
[2]NTT Network Innovation Laboratories, NTT Corporation, 1-1 Hikarino Oka, Yokosuka, Kanagawa 239-0847, Japan
[3]NTT Device Technology Laboratories, NTT Corporation, 3-1 Morinosato Wakamiya, Atsugi, Kanagawa 243-0198, Japan
[4]NTT Innovative Devices Corporation, 1-1-32 Shin Urashima, Yokohama, Kanagawa 221-0031, Japan
[5]Finisar Australia Pty Ltd, Rosebery, NSW 2018, Australia
Author e-mail address:kny.suzuki@ntt.com

Abstract: We propose double-decker ROADM node by introducing a band cross-connect in addition to the conventional wavelength cross-connect, which is suitable for a multi-band network. This configuration provides improved transmission characteristics compared with a conventional CDC-ROADM. © 2024 The Author(s)

1. Introduction

Advances in mobile infrastructure, cloud services and artificial intelligence technology require high-capacity communications in carrier networks as well as between data centers. In particular, when considering large-scale datacenters, it can be envisioned that the communication demand will reach and exceed the capacity limit of a single band, whereas the capacity of a single band and the improvement of spectral efficiency appear to have saturated in recent years. To expand the capacity of a single optical fiber transmission, the deployment of C+L-band transmission is underway, and furthermore, multi-band systems with three or more bands have actively been reported from various perspectives including the transmission characteristics [1,2], network and node architecture [3–6], and devices [7,8]. Regarding C+L-band colorless, directionless, and contentionless (CDC)-ROADM nodes, we have proposed node configurations characterized by band-continuous or band-unaware features that provide network operators the benefit of improved operability [9–11]. For such large-scale data center interconnections, establishing optical paths on a wavelength-by-wavelength basis may not be necessary in a multi-band system. Instead, band-by-band routing is appropriate [6]. One of the requirements for such high-capacity interconnections, is that the transmission lines and associated equipment should be as transparent as possible to maintain high signal quality at the point of transmission, thereby maximizing transmission capacity and distance. This paper proposes a double-decker CDC-ROADM node that consists of a wavelength cross-connect with wavelength granularity and a band cross-connect with band granularity. It is a practical implementation for a multi-band node that possesses the necessary and sufficient functionality of a CDC-ROADM. We experimentally demonstrated that the band cross-connect is effective to improve the transmission quality of nodes using >1 Tbps net bit rate (NBR) signals with 144-Gbaud dual polarization (DP) 64-QAM signals.

2. Double-decker ROADM node

2.1. Node configuration

Figure 1 shows the schematic configuration of the proposed double-decker ROADM node. It consists of a wavelength cross-connect on the first layer and a band cross-connect on the second layer. The band cross-connect directly routes

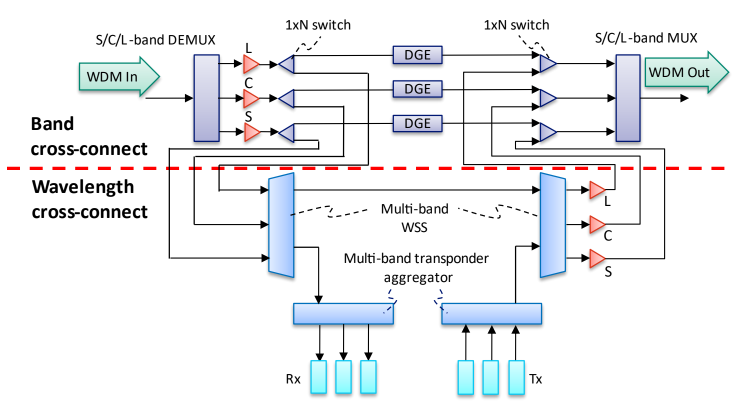

Fig. 1 Double-decker node architecture for multi-band ROADM system consisting of band- and wavelength cross-connect.

the demultiplexed bands from the ingress to the egress at the band granularity. In contrast, the wavelength cross-connect handles the wavelength signals to be added/dropped and their multiplexing with expressing wavelengths. The CDC-ROADM functionality is assured by the first layer wavelength connections. The key components in the band cross-connect are the S/C/L-band (de)mux filters, 1×N switches, dynamic gain equalizing filters (DGE) and a single-stage of optical amplifiers, while the wavelength cross-connect requires multi-band wavelength selective switches (WSSs) and multi-band transponder aggregating multicast switches. The essence of the band cross-connect is that it utilizes devices with simple functionality, which have smaller insertion losses than those in the wavelength cross-connect and provides an advantage of improved transmission characteristics. In general, when an optical signal is amplified by rare-earth-doped amplifiers, the signal-to-noise ratio of the signal degrades, resulting in inferior signal quality. The low-loss band cross-connect can omit a set of booster optical amplifiers, as shown in Fig. 1. Therefore, the transmission capacity and the achievable distance can be enhanced when the band is provisioned on a band-by-band basis.

2.2. Key components for double-decker ROADM

To make the best use of wavelength resources, continuous allocation of wavelength channels among bands is preferable. However, at this point, it is difficult to develop an optical amplifier that covers multiple bands with a single unit. Thus, band-division-multiplexed (BDM) signals need to be divided into separate bands in which a single-band optical amplifier can be implemented. Even though for band demultiplexing, narrow band boundaries are preferable for the effective use of wavelength resources. Narrow guard-band S/C/L-band (de)mux filters were developed that consisted of tandemly connected arrayed-waveguide gratings (AWG) [12] with extremely high resolution using a silica-based planar lightwave circuit (PLC), as shown in Fig. 2 [13]. The first stage AWG demultiplexes the input BDM signal into 150-GHz components, and the second stage multiplexes these signals on a band-by-band basis. Thus, the guard-band can be reduced to 150 GHz, whereas the band boundaries of conventional thin-film filters are as wide as several nano meters.

Spectral equalization may be necessary to compensate for the spectral slope caused by wavelength-dependent loss in the fiber and stimulated Raman scattering (SRS)-induced power transfer among bands. DGEs should be arranged in between 1×N switches on the ingress and egress sides in the band cross-connect, whereas the WSSs function as channel equalizers with their variable optical attenuating function in the wavelength cross-connect. The DGEs need to compensate not for a complex non-flattened spectrum but for a simple linear spectrum slope, because built-in gain flattening filters equalize the complex spectra. Instead, it is important for DGEs to have low insertion loss characteristics. Therefore, we fabricated a lattice-form filter, composed of cascaded Mach-Zehender interferometers (MZI) using silica-based PLC technology as shown in Fig. 3 (a) [14]. We integrated three sets of 5-stage lattice filters with path length differences of 0.5, 10, 0.5, 20 and 0.5 µm, respectively. Figure 3 (b) shows an equalized spectrum of the S-band signal. The insertion loss of the DGE is less than 3 dB, including the principle loss of compensation.

Optical switches play a crucial role for both layers. In the wavelength cross-connect, multi-band WSSs [15] are essential. Another class of switches that form the wavelength cross-connect includes multi-band transponder aggregating switches [10,11]. To demonstrate the proposed ROADM node, we developed a new multi-band multicast switch, which operates over S to L bands that consists of broadband power-splitting couplers and all-band MZI with silica-based PLC technology [8]. In the band cross-connect, it is important that 1×N switches have low loss. The switch scale N equals the number of node degrees, typically 8~16 or several times more if BDM is combined with space-division multiplexing in the future. Silica-based PLC is suitable to provide switches with such scale and low-loss characteristics, achieving less than 2 dB of insertion loss.

2.3. Experiment

Figure 4 (a) shows the experimental setup for the node with narrow guard-band S/C/L-band (de)mux filters, DGE and 1×N switches mentioned in the previous section. In the wavelength cross-connect, the C+L-band WSS [15] and S-

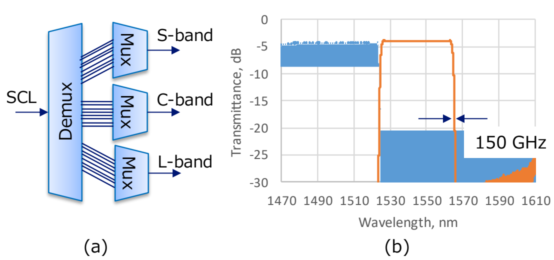

Fig. 2 Narrow guard-band S/C/L (de)mux filter. (a) Functional block and (b) demultiplex spectra

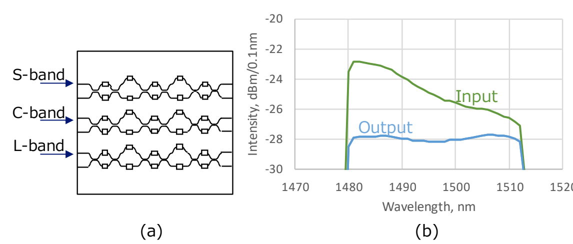

Fig. 3 Dynamic gain equalizer. (a) Schematic diagram and (b) equalization spectra for a tilt spectrum in S-band.

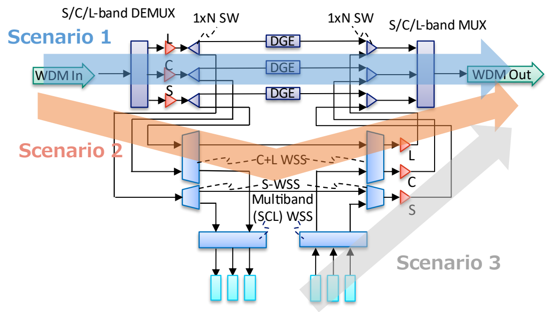

(a)

Band	Input power, dBm/λ	Wavelength, nm	Frequency, THz
S	-11.3	1482.287	202.250
		1495.597	200.450
		1510.290	198.500
C	-11.8	1529.944	195.950
		1545.322	194.000
		1562.233	191.900
L	-12.3	1572.063	190.700
		1589.568	188.600
		1607.466	186.500

(b)

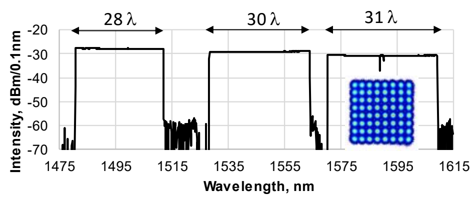

(c)

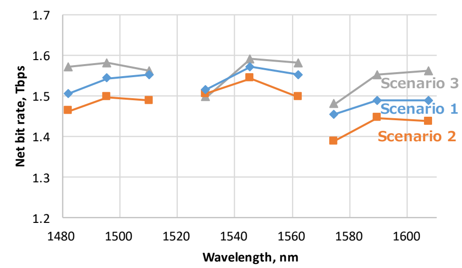

(d)

Fig. 4 Experiment. (a) Experimental setup and test scenarios, (b) test signal wavelengths, (c) test signal spectra, and (d) measured net bit rate.

band WaveShaper 4000A were used as multi-band WSSs [16]. We measured the NBR using a required code rate derived from the rate-adaptive coding technique [1] at nine wavelengths shown in the table in Fig. 4 (b), which are located at the center, shorter, and longer edges of the S-, C-, and L-bands. The measurement was performed using the same setup as described in [1], except for a 101-km fiber and Raman pumps. The signals were DP 64-QAM ones of around 1.6-Tbps-NBR with a baud rate of 144 Gbaud and a channel spacing of 150-GHz. Amplified spontaneous emissions for three bands were multiplexed and input to emulate full WDM signals. The emulated numbers of channels were 28, 30, and 31 for the S-, C-, and L-bands, respectively, as shown in Fig. 4 (c). A typical constellation is shown in the inset. The band boundaries had large gaps because of optical amplifiers and DGE operational wavelength limitations, despite the narrow 150-GHz guard-bands of the S/C/L-band (de)mux filters. The measurement was performed with three scenarios: Scenario 1 involved band cross-connect transmission, scenario 2 covered wavelength cross-connect transmission, and Scenario 3 included signal addition from the add port to the egress port. The measured NBRs are plotted in Fig. 4 (d). As expected, NBRs for the band cross-connect (blue plots) exceeded those for the wavelength cross-connect (orange plots) for all the wavelength channels. The added signals (grey plots) showed the best NBR except for the shortest signal in the C-band. This was because the signal powers output from the transmitter were high enough while the shortest signal in C-band had in-band tilt. The degradations in the shortest signal in the L-band for all scenarios were also caused by the in-band. The experimental result indicates that our proposed band cross-connect contributes to improve signal quality compared with conventional wavelength crossconnect.

3. Conclusion

We proposed a double-decker ROADM node configuration that combines the band cross-connect and wavelength cross-connect for a multi-band network, and described the devices needed to construct the node. We also experimentally proved that introducing the band cross-connect effectively improves the transmission quality of the node experimentally. This proposal has the potential to improve the transmission quality and/or to extend the reach in large-capacity multi-band CDC-ROADM systems.

Acknowledgement

The authors would like to thank Coherent Inc. for providing S-band WaveShaper in the experiment.

References

[1] F. Hamaoka, *et al.*, *in Proc. OFC23*, Th3F.2 (2023).
[2] A. Ferrari, *et al.*, *J. Lightw. Technol.* 38 (16), 4279-4291 (2020).
[3] M.S. Sarwar, *et al.*, *in Proc. OFC20*, M2G.6 (2020)
[4] M. Nakagawa, *et al.*, *in Proc. OFC22*, W2A.24 (2022)
[5] J.F.O. Ramos, *et al.*, *in Proc. ICTON23*, Th.A4.5 (2023)
[6] H. Hasegawa, *IEICE Trans. Commun.*, DOI:10.1587/transcom.2023PNI0002
[7] R. Kraemer, *et al.*, *J. Lightw. Technol.*, 29 (19), 6023-6032 (2021)
[8] T. Goh, *et al.*, *in Proc. OFC22*, paper W4B.1. (2022)
[9] Y. Yiran, *et al.*, *in Proc. OFC19*, M1A.3, (2019).
[10] S. Yamamoto, *et al.*, *Opt. Express* 29, 36353-36365 (2021)
[11] K. Suzuki, *et al.*, *J. Lightw. Technol.*, 41(10), 3074-3083 (2023)
[12] C. R. Doerr, *et al.*, *Photon. Technol. Lett.*, 15 (8), 1088-1090 (2023).
[13] M. Ota, *et al.*, submitted to *OFC24.*
[14] Y. Morimoto, *et al.*, *in Proc. IEICE soc. conf.*, C-3/4-15 (2022).
[15] https://www.lightwaveonline.com/test/design-manufacturing/article/14199805/finisar-wss-flexgridr-cl-wavelength-selective-switch
[16] https://www.coherent.com/networking/optical-instrumentation/waveshaper